Contents lists available at ScienceDirect

Chemical Engineering Research and Design

journal homepage: www.elsevier.com/locate/cherd

Continuous slug flow crystallization: Impact of design and operating parameters on product quality

*Maren Termühlen, Matthias Markus Etmanski, Ines Kryschewski, Anne Cathrine Kufner, Gerhard Schembecker, Kerstin Wohlgemuth**

ARTICLE INFO

Article history:
Received 9 February 2021
Received in revised form 3 April 2021
Accepted 10 April 2021
Available online 18 April 2021

Keywords:
Continuous crystallization
Slug flow crystallization
Product quality
Crystal size distribution
Agglomeration

ABSTRACT

A slug flow crystallizer for cooling crystallization with focus on enhanced product quality control in terms of narrow particle size distribution (PSD) was designed and characterized. Emphasis was put on slug flow stability while maintaining a convex shape of slugs to make use of the advantage of a narrow residence time distribution. Measurements of the latter one showed plug-flow-like behavior for the liquid and solid phase independent of the operating conditions within the range investigated. A tube-in-tube temperature concept led to smooth cooling from 50 to 31 °C avoiding supersaturation peaks. Seeded cooling crystallization of aqueous L-alanine solution successfully led to reproducible product PSDs avoiding secondary nucleation. Thereby the crystals' median diameter was increased by 240 μm. Within a residence time of 10.5 min only, a relative process yield of approximately 83% was achieved. To identify optimized operating conditions for narrow PSD and reduced agglomeration, the effect of total volume flow rate, slug length, and cooling rate on the PSD and agglomeration degree was quantified. A high flow rate (40 mL min^{-1}) and a high cooling rate (3.6 K min^{-1}) reduced agglomeration to its minimum and shifted the size distribution of single crystals without its broadening by in average 90 μm.

1. Introduction

In the field of pharmaceutical and fine chemical industry, one characteristic for a successful crystallization process is seen in obtaining a specific and controllable crystalline product quality, including, e.g., particle size and its distribution, morphology, and agglomeration degree (Yazdanpanah and Nagy, 2020; Liu and Nagy, 2020). Compared to the well-known batch crystallization, small-scale continuous crystallizers offer the advantages of higher process efficiency by simultaneously using smaller apparatuses, and higher reproducibility of the product quality due to operation at steady state (Yazdanpanah and Nagy, 2020; Jiang and Braatz, 2018; Wood et al., 2019; Wang et al., 2017; Zhang et al., 2017).

In the past years, lots of research was performed developing small-scale continuous crystallizers to improve either the process itself or the crystalline product properties (Wood et al., 2019; Zhang et al., 2017; Wang et al., 2017; Jiang and Braatz, 2018; Nagy et al., 2020). In general, two types of crystallizers can be identified (Chen et al., 2011): Mixed suspension mixed product removal (MSMPR) and tubular crystallizers. MSMPR crystallizers as continuously stirred tanks, already intensively investigated within academic research (Wood et al., 2019; Zhang et al., 2017; Wang et al., 2017; Lührmann et al., 2018;

Abbreviations: ag, aggregated/agglomerated crystal; CM, cooling medium; FEP, fluorinated-ethylene-propylene; FFT, Fast Fourier transform; MSMPR, mixed suspension mixed product removal; PM, process medium; PSD, particle size distribution; PVC, polyvinyl chloride; RTD, residence time distribution; RTD_L, residence time distribution of liquid phase; RTD_S, residence time distribution of solid phase; sc, single crystal; SFC, slug flow crystallizer; TM, tempering medium.

* *Corresponding author.*
E-mail address: kerstin.wohlgemuth@tu-dortmund.de (K. Wohlgemuth).

https://doi.org/10.1016/j.cherd.2021.04.006

Nomenclature

Bo	Bodenstein number [–]
c	concentration [$g_{alanine}\ g_{sol}^{-1}$]
c^*	saturation concentration [$g_{alanine}\ g_{sol}^{-1}$]
d_i	equivalent diameter [μm]
d_i	inner diameter [mm]
$d_{50,3}$	volumetric based median crystal size [μm]
$E(t)$	exit age distribution [–]
$F(t)$	cumlative residence time distribution [–]
L_{tubing}	tubing length [m]
n	stirring rate [rpm]
p	pressure [bar]
$Q_{Air,0}$	synthetic air volume flow rate at slug formation [mL min^{-1}]
Q_{Liq}	liquid's volume flow rate [mL min^{-1}]
$Q_{Susp,0}$	suspension's volume flow rate [mL min^{-1}]
Q_{tot}	total volume flow rate [mL min^{-1}]
t	time [s]
$\bar{t}$	mean residence time [s]
v	velocity [mm s^{-1}]
V	volume [mL]
w_{Solid}	mass based solid content [%$g_{Solid}\ g_{Sol}^{-1}$]
Y_{rel}	relative process yield [%]
$\epsilon_{L,0}$	liquid hold-up at slug formation [–]
η_G	dynamic viscosity of gaseous phase [mPa s]
η_{sol}	dynamic viscosity of solution [mPa s]
ϑ	temperature [°C]
ϑ^*	saturation temperature [°C]
$\Theta_{FEP,H_2O,air}$	three-phase contact angle [°]
Θ	normalized residence time [–]
ρ_G	density of gaseous phase [kg m^{-3}]
ρ_{sol}	density of solution [kg m^{-3}]
σ_{sol}	surface tension [N m^{-1}]
σ	variance [s]
τ	hydrodynamic residence time [s]

Alvarez et al., 2011), allow long residence times useful for slow crystal growth kinetics. However, a broad residence time distribution (RTD) has to be accepted, which can lead to a broad particle size distribution (PSD). Regarding tubular crystallizers, the benefit of a plug-flow-like narrow RTD can only be used when operated under turbulent flow. This flow regime, however, leads to high flow velocities and, thus, to very short residence times as the pressure drop limits the crystallizer length (Liu and Nagy, 2020). An operation under laminar flow increases the residence time, but also comes along with a broader RTD and entailing broader PSD as well as increased probability for fouling and clogging (Jiang et al., 2014; Eder et al., 2012). Hence, over the years, innovative concepts aiming for long residence times and narrow RTD were introduced to the field of crystallization. Different apparatuses, like crystallizers using static mixers (Alvarez and Myerson, 2010), helically coiled (Wiedmeyer et al., 2017) or coiled flow inverted tubular crystallizers (Hohmann et al., 2016, 2018), continuous oscillatory baffled crystallizers (Lawton et al., 2009; Briggs et al., 2015; Kacker et al., 2017, 2018), or slug flow crystallizers (Jiang et al., 2014, 2015; Mou et al., 2019; Mou and Jiang, 2020; Su and Gao, 2018; Wittering, 2015; Robertson et al., 2016; Levenstein et al., 2020) came up.

Thereby, the slug flow crystallizer (SFC) stands out due to its two-phase flow. The principle is as follows: The mother liquor is segmented by an immiscible segmentation medium into so-called slugs being well-mixed due to internal circulations caused by the no slip condition at the inner tubing wall. Originating from the field of reaction engineering (Scheiff and Fluiddynamik, 2015; Jongen et al., 2003; Kubo et al., 1998; Guillemet-Fritsch et al., 2004), the segmented flow provides promising features such as minimized axial dispersion (Thulasidas et al., 1995) and enhanced solid suspension reducing the risk for fouling and clogging compared to single-phase flow. The superior heat transfer attracts the slug flow crystallizer for application in cooling crystallization.

In literature, several SFCs have been investigated (Jiang et al., 2014; Jiang and Braatz, 2018; Mou and Jiang, 2020; Robertson et al., 2016; Neugebauer and Khinast, 2015; Neugebauer et al., 2018; Su and Gao, 2018; Eder et al., 2012; Wittering, 2015; Levenstein et al., 2020; Wang et al., 2018; Hadiwinoto et al., 2019). An essential distinction must be made between liquid-liquid (Wittering, 2015; Robertson et al., 2016) and gas-liquid operation (Jiang et al., 2014; Mou et al., 2019; Eder et al., 2012; Neugebauer and Khinast, 2015; Su and Gao, 2018), with, e.g., air as gas supply. Whilst the use of air leads to an easier product separation at the end of the crystallization process, utilizing a liquid phase can enhance the stability of slug flow for particular substance systems (Wittering, 2015). However, the risk of contamination due to cross solubility and the need for an additional separation unit leads to air as segmentation medium in most cases (Eder et al., 2012; Neugebauer and Khinast, 2015; Besenhard et al., 2017; Neugebauer et al., 2018; Jiang et al., 2014, 2015; Mou et al., 2019; Mou and Jiang, 2020; Lu et al., 2015; Su and Gao, 2018).

The stability of slug flow bears a challenge for the design and operation of an SFC and depends on different parameters: The slug flow regime is characterized by the dominance of surface forces over gravitational forces (Ghiaasiaan and Abdel-Khalik, 2001). Hence, respective inner diameters for continuously operated SFCs in literature vary between 2 mm and 4.6 mm, as the impact of surface forces is increased for small diameters (Neugebauer et al., 2018; Mou and Jiang, 2020; Wittering, 2015).

Fluid properties like density and interfacial tension combined with the wettability properties of the tubing material used are decisive parameters for a successful crystallization process. Su and Gao (2018) investigated the influence of different tubing materials on the decrease of supersaturation crystallizing glycine from aqueous solution. Wang et al. (2020) observed severe wall crystallization facilitating the risk of clogging inside tubing materials like silicone or polyvinyl chloride (PVC) (Wang et al., 2020). By using a hydrophobic tubing material for crystallization of a hydrophilic substance system, the presence of a liquid wall film can be avoided for air-liquid segmented flow minimizing the risk for encrustations (Jiang and Braatz, 2018; Su and Gao, 2018). Hence, for decreasing wettability of the liquid phase to be crystallized, the three phase contact angle of the two fluids and the tubing should be increased (Günther and Jensen, 2006).

Next to encrustation issues, the slug's shape formed might have an impact on the RTD. SFCs are claimed to have a narrow RTD (Besenhard et al., 2017; Jiang et al., 2014; Jiang and Braatz, 2019; Yazdanpanah and Nagy, 2020). However, for substance systems leading to a wall film (concave slugs), e.g., using ethanol as solvent and silicone as tubing material, Besenhard et al. (2017) could observe crystals traveling between adjacent slugs. Thus, the SFC's major advantage of minimizing axial dispersion enabling a narrow PSD diminishes. To the best of

our knowledge, only the liquid phase's RTD (RTD_L) has been quantified for a microchannel slug flow reactor, until now (Trachsel et al., 2005). However, for crystallization processes focusing on a narrow PSD, the knowledge of the solid phase's RTD (RTD_S), is of special interest.

Especially in cooling crystallization, the control of temperature over length of a tubular crystallizer becomes decisive as it directly determines supersaturation. In literature, cooling is achieved by using natural cooling with air (Mou et al., 2019; Jiang et al., 2015) or water baths (Mou et al., 2019; Robertson et al., 2016; Besenhard et al., 2017; Neugebauer et al., 2018; Kudo and Takiyama, 2012; Hadiwinoto et al., 2019). However, in both cases, a smooth cooling as desired for a controlled crystallization process becomes challenging. In case of using natural cooling at ambient temperatures, the process medium's temperature is drastically decreased at the tubing's beginning resulting in supersaturation peaks. Furthermore, the cooling rate is not adjustable limiting the operating window for controlled crystallization. When using water baths, temperature steps are realizable, only. This can be advantageous regarding modification on crystal shape or polymorphic form by temperature cycling, which recent publications focused on (Neugebauer et al., 2018; Besenhard et al., 2017; Levenstein et al., 2020). However, temperature steps also induce supersaturation peaks especially at the tubing's inlet, which should be avoided (Rasche et al., 2016). Hence, for a controlled crystallization process, many of those temperature steps are needed resulting in many water baths and increasing investment costs. Contrary to that, Rasche et al. (2016) showed in their simulations that a counter-current double-pipe heat exchange, often used in industrial applications, enables a smooth temperature profile and thus, step-less generation of supersaturation. However, none of the slug flow crystallizers in literature are equipped with such a heat exchange concept.

Due to the promising advantage of a narrow RTD, several researchers focused on the particle size and its distribution obtained from crystallization inside SFC (Jiang et al., 2014, 2015; Neugebauer and Khinast, 2015; Su and Gao, 2018). Different nucleation methods, like seeding, ultrasonication, impinging jets, or ice crashed cooling were investigated (Jiang et al., 2015, 2014; Eder et al., 2012; Su and Gao, 2018; Mou and Jiang, 2020). A spatially separated nucleation and crystal growth zone enhanced product quality control obtaining a narrower PSD (Jiang et al., 2014; Neugebauer and Khinast, 2015). Much work was done regarding optimal operating parameters for the nucleation zone to reproducibly generate seeds with a narrow PSD (Jiang et al., 2014; Mou and Jiang, 2020). However, concerning the slug flow zone, in most cases, constant operating conditions, like total volume flow rate or phase ratio, were chosen and the impact of these conditions inside the slug flow zone has not been investigated until now.

This study aims at the design and operation of a slug flow crystallizer for enhanced product quality control meaning a narrow particle size distribution and an increased process yield. These two aims can only be met when the following requirements are fulfilled:

- Narrow RTD, especially RTD_S, to enable equal crystal growth conditions
- Smooth cooling profile to enable a smooth supersaturation profile avoiding secondary nucleation
- Spatial separation of nucleation and crystal growth (Jiang et al., 2014)
- Increased residence time for high process yield
- Efficient suspension of particles in slug flow zone to minimize agglomeration

In a first part of this work, measurements of the liquid and solid phase RTD are conducted. A tube-in-tube cooling concept is implemented, aiming for a smooth cooling over the tubing's length to avoid supersaturation peaks. With respect to the aims of obtaining a narrow product PSD along with an increased process yield, an optimal operating window is determined. Knowing that, e.g., the volume flow rate has opposing effects on suspension and residence time, which might impact the two aims mentioned above, the effect of different operating parameters like slug length, slug velocity, or cooling rate on the PSD is quantified. As the PSD alone does not allow any insights into the degree of particles' agglomeration (Terdenge and Wohlgemuth, 2016; Heisel et al., 2018), a special focus is set on the distinction of single crystals (sc) and aggregated/agglomerated crystals (ag) in this study. With this knowledge, optimized operating conditions with respect to a narrow PSD and minimized aggregation/agglomeration degree are determined.

2. Material and methods

2.1. Systems investigated

For the generation of a gas-liquid segmented flow, in all experiments synthetic air ($\rho_G = 1.18\,kg\,m^{-3}$, $\eta_G = 18.24 \cdot 10^{-3}\,mPa\,s$) represented the gaseous phase. The air was saturated with the respective solvent prior to slug formation to avoid solvent's evaporation into the air bubbles. For the measurement of the liquid phase's RTD, a solution of ultrapure water (Mili-Q Integral System, $0.05\,\mu S\,cm^{-1}$) mixed with methylene blue (Merck KGaA, $\sigma_{MB,0.015\,g\,L^{-1}} = 72.2 \cdot 10^{-3}\,N\,m^{-1}$) with a concentration of $c_{MB} = 0.015\,g\,L^{-1}$ was chosen as tracer substance. For the measurement of the solid phase's RTD, recrystallized L-alanine crystals, previously sieved within a range of 250–315 μm ($d_{50,3} = 300\,\mu m$, $d_{90-10,3} = 232\,\mu m$), were resuspended in a saturated solution of L-alanine/ water ($\rho_{Sol} = 1043\,kg\,m^{-3}$, $\eta_{Sol} = 1.61\,mPa\,s$, $\sigma_{Sol} = 66.7 \cdot 10^{-3}\,N\,m^{-1}$) at an ambient temperature of $\vartheta^* \approx 22\,^{\circ}C$. Thereby, the crystals were prepared according to the procedure from Ostermann et al. (2018). The solubility curve of L-alanine (Evonik Industries AG, 99.6% purity) is described by Eq. (1) (Wohlgemuth, 2012).

$$c\left(g_{alanine}\,g_{sol}^{-1}\right) = 0.11238 \cdot \exp\left(9.0849 \cdot 10^{-3} \cdot \vartheta^*\,(^{\circ}C)\right) \quad (1)$$

For the seeded crystallization experiments, an aqueous L-alanine solution was prepared at a saturation temperature of $\vartheta^* = 50\,^{\circ}C$. Recrystallized L-alanine crystals (Ostermann et al., 2018) within a sieving range of 160–200 μm ($d_{50,3} = 281\,\mu m$, $d_{90-10,3} = 135\,\mu m$) were added to the saturated solution.

2.2. Experimental setup

The promising advantages of an SFC can only be utilized when the slugs show convex shape. Hence, for the polar substance system L-alanine/water to be crystallized a hydrophobic tubing material consisting of fluorinated-ethylene-propylene (FEP from Nalgene, $\Theta_{FEP}, H_2O, air = 109^{\circ}$) was chosen with an inner tubing diameter of $d_{i,tubing} = 3.18\,mm$ ($d_{out,tubing} = 4.76\,mm$). Advantageously, when placed into water, this material becomes transparent such that the stability and shape of

slug flow can be investigated non-invasively via image-based analytics (Termühlen et al., 2019). Regarding the measurement of the RTDs and the development of the cooling strategy, a prototype SFC with a tubing length of $L_{tubing} = 7$ m was used. However, for later crystallization experiments in which an increased residence time for crystal growth is needed, this length was extended resulting in tubing lengths varying from 13.25 m up to 26.5 m (see Section 3.3).

Depending upon the experiments conducted (see following sections), the feed either originated from the feed solution tank (V = 2.5 L) or the feed suspension tank (V = 450 mL) (see Fig. 1, for real image see Fig. S1 in Supporting Information). In case of the suspension as feed, two aspects had to be kept in mind: First, the suspension inside the tank needed to be stirred as homogeneously as possible, which was realized with a cone at the bottom of the tank following the design procedure stated by Lührmann et al. (2018). Second, this tank needed to be placed as vertical as possible above the peristaltic pump and the following T-junction for slug formation. Due to laminar flow inside the periphery, the suspension's crystals tended to settle, which had to be avoided to guarantee a constant feed's solid content.

A peristaltic pump (Ismatec Reglo Digital MS-4/12, $d_{i,tubing} = 2.29$ mm Pharmed) either pumped the solution or the suspension towards the slug formation zone. To pump the suspension containing crystals up to a median diameter of $d_{50,3} = 300\,\mu m$, only two of the four channels available were used, increasing the flow velocity inside the pump tubings to avoid clogging issues.

The slug flow was formed hydrodynamically with the solution or suspension and synthetic air. Thereby, in our previous work, we could show that inside a hydrophobic T-junction made of polypropylene ($d_i = 3.18$ mm) slugs with a narrow slug length distribution are formed (Termühlen et al., 2019). The solution's mass flow rate was measured gravimetrically and recalculated to the volume flow rate, two times just before experiment's start and for validation once after experiment's end. The synthetic air was directly supplied via pipeline pressure from a gas cylinder, according to the procedure described in our previous study (Termühlen et al., 2019). Due to pressure drop along the tubing length of the slug flow zone and the compressibility of air, its volume flow rate needed to be adjusted according to a recalculation with the help of the ideal gas equation. The phase's ratio at the slug formation (variable index 0) was described with the help of the liquid hold up $\epsilon_{L,0}$ defined by the volume flow rates of the liquid $Q_{Liq,0}$ and air $Q_{Air,0}$. By varying $\epsilon_{L,0}$, the slug length can be manipulated (Termühlen et al., 2019).

$$\epsilon_{L,0} = \frac{Q_{Liq,0}}{Q_{tot}} \approx \frac{Q_{Liq,0}}{Q_{Liq,0} + Q_{Air,0}} \tag{2}$$

In order to ensure isothermal conditions or to enable polythermal cooling for the crystallization experiments, a tube-in-tube cooling concept was realized (see Section 3.2). The SFC's tubing was jacketed with an outer tubing made of PVC for transparency reason ($d_{i,PVC} = 15$ mm). With the help of a thermostat (Haake CC-K6), tempered water was pumped through the PVC tubing jacketing the slug flow tubing. To ensure an equal heat transfer along the whole SFC, an even flow of the tempered water around the inner tubing had to be realized. For this purpose, every 0.5 m internal spacers were installed to keep the slug flow tubing centered towards its outer tubing. A throttle and a bypass of the tempered water enabled the adjustment of different volume flow rates for polythermal cooling (see Section 3.2). The temperature profile was measured with the help of temperature sensors Pt100 (class A; experimental deviation of $0.15 + 0.002 \cdot \vartheta\ [^\circ C]$).

In all experiments conducted, a steady state was obtained before any samples for PSD measurement or videos for slug flow stability were taken (Termühlen et al., 2019). A steady state was achieved when the temperature profile and the pressure at slug formation remained constant which led to the conclusion of a stable slug flow over tubing's length. Repetitions of the respective experiments (see Supporting Information Table S2) showed that these steady state conditions (constant pressure and temperature profile) lead to reproducible PSDs.

2.3. Experimental procedures

2.3.1. Liquid and solid phase's residence time distribution

As already explained in Section 1, the advantage of the SFC's narrow RTD can only be fully utilized when the slugs show convex shape such that the formation of a wall film is avoided. Therefore, RTD_L and RTD_S measurements were conducted. For this, the slug flow crystallizer, shown in Fig. 1, with a tubing length of $L = 7$ m was used.

For both RTDs, a step response was measured. Hence, the cumulative residence time distribution, also known as F curve, results from this measurement representing the fraction of all volume elements that have in sum already left the slug flow zone at the particular normalized time Θ (see Eq. (3)) (Nauman, 2004). The exit age distribution, also known as E curve, stating the fraction of volume elements that leave the SFC at the specific time point t, can be obtained by differentiation (see Eq. (4)).

$$\Theta = \frac{t}{\tau} \tag{3}$$

$$E(t) = \frac{dF(t)}{dt} \tag{4}$$

With the help of the Bodenstein number (Bo) relating convection to axial dispersion, real flow tubes can be characterized in order to attribute them either towards the back mixing behavior of a stirred tank (Bo = 0) or towards an ideal plug flow tube (Bo = ∞) (Baerns, 2013). The model of an ideal plug flow can be applied for Bo > 100 and, thus, be simplified (Baerns, 2013). Therewith, the Bodenstein number can be calculated with the hydrodynamic residence time τ and the variance σ around the mean residence time $\bar{t}$ (see Eqs. (5)–(8)) (Baerns, 2013).

$$Bo = \frac{2\,\tau^2}{\sigma^2} \tag{5}$$

$$\tau = \frac{V_{SFC}}{Q_{tot}} \tag{6}$$

$$\sigma^2 = \int_0^\infty \left(t - \bar{t}\right)^2 E(t)\,dt \tag{7}$$

$$\bar{t} = \int_0^\infty t\,E(t)\,dt \tag{8}$$

For the RTD_L measurement the feed solution vessel was filled with deionized ultrapure water, whilst the feed suspension vessel was filled with the tracer solution of water and methy-

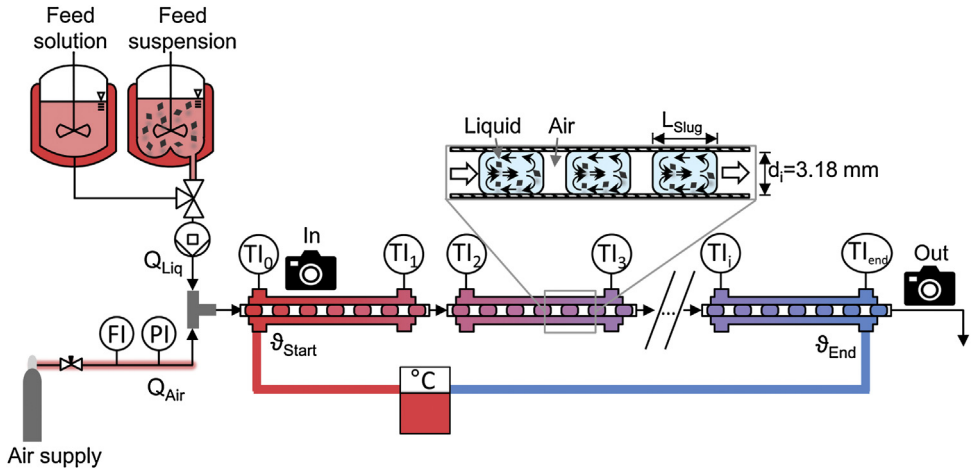

Fig. 1 – Schematic depiction of setup. The slug flow's tubing length varied from 7 m up to 26.5 m depending upon the experiment conducted.

lene blue. Both were stirred with a stirring rate of $n = 300$ rpm at ambient temperature of $\vartheta \approx 22\,^{\circ}C$ (see Section 2.1 and Fig. 1). A concentration of $c_{MB} = 0.015\,g\,L^{-1}$ was used to ensure a linear correlation between the change in mean brightness as signal measured and the concentration. After reaching steady-state in the slug flow zone (Termühlen et al., 2019), operated with air-water segmented flow, the three-way-valve (see Fig. 1) was switched, and the tracer solution was pumped to the slug flow zone to initiate the measurement of a step response. Thereby, the segmented flow represents a challenge when it comes to measurement of the change in signal. Common techniques, like conductivity measurement, require the use of a probe leading to disturbance of the slug flow. However, non-invasive image based analytics allowed the investigation directly at the beginning of the slug flow zone and its end while maintaining slug flow stability (see Fig. 1).

For evaluating the videos taken, the change in mean brightness was used to quantify the step response. For that an automated method was developed (see Supporting Information): The videos were cut into images such that a particular column of the image's matrix was evaluated to detect a change in brightness whenever the blue color exceeded this column (see Figs. S2, S3 and S4 in Supporting Information). By recording in- and outlet of the SFC coincidently, a deconvolution of the two signals with the help of Fast Fourier transform (FFT) becomes possible such that the pure transfer function of the slug flow zone without influence of the periphery was quantified (see Eq. (9)) (Trachsel et al., 2005).

$$E_{deconv}(\Theta) = \mathrm{FFT}^{-1}\left(\frac{\mathrm{FFT}\,(E_{out}\,(\Theta))}{\mathrm{FFT}\,(E_{in}\,(\Theta))}\right) \tag{9}$$

The RTD_L was measured for total volume flow rates $Q_{tot} = 30$–$60\,mL\,min^{-1}$ and liquid hold ups $\epsilon_{L,0} = 0.33$–0.66. These parameter ranges were identified as possible operating window before (Termühlen et al., 2019).

Recrystallized L-alanine crystals with a diameter of $d_{50,3} = 300\,\mu m$ were resuspended in saturated aqueous solution with a solid content of $5.13\%\,g_{Ala}\,g_{Sol}^{-1}$ representing the yield for a possible cooling crystallization from 50 to 20 °C. In order to guarantee a feed with constant solid content, this suspension was stirred with a stirring rate of $n = 450$ rpm to ensure homogeneous distribution of crystals inside the suspension vessel (see Fig. 1). Again, with the three-way valve and the aforementioned pump, the suspension was transferred to the slug formation.

For the RTD_S measurement, a gravimetrical approach was chosen. For that, samples were continuously taken at the end of the slug flow zone. The slugs were manually collected in small sample vessels for approx. 5 s each. To track the change in solid content as measure for the RTD_S precisely, the sample volumes within the sampling time of 5 s should be small. This could be achieved for small volume flow rates and low liquid hold ups ($Q_{tot} = 30\,mL\,min^{-1}$, $\epsilon_{L,0} = 0.33$). The samples were dried for 48 h at 50 °C in a vacuum drying oven (Thermo Scientific Heraeus VT 6130).

2.3.2. *Cooling crystallization*

For the separation of nucleation and growth zone, seeding was chosen as nucleation method as it enables the possibility to quantify the performance of the slug flow zone as growth zone only. An aqueous L-alanine solution at saturation temperature of $\vartheta^* = 50\,^{\circ}C$ was prepared inside the feed suspension tank ($V = 450\,mL$). Meanwhile, the slug flow zone was started up with air-water segmented flow.

According to heuristic rules from batch crystallization, Beckmann (2013) stated that an addition of 0.1–1 wt.-% of seed crystals should be used in order to control the crystallization process. From preliminary experiments (see Supporting Information Fig. S8) the seed loading was determined to 1% $g_{ala}\,g_{sol}^{-1}$ to suppress the influence of secondary nucleation to follow the aim of separating nucleation from crystal growth. To ensure a large surface area, small seed crystals, previously sieved in a range of 160–200 μm, were used. After reaching steady state in slug flow as well as in the temperature profile, these recrystallized crystals were resuspended at a stirring rate of $n = 450$ rpm. The feed suspension tank was kept tempered at $\vartheta = 50\,^{\circ}C$ to avoid crystal growth or agglomeration (see Fig. 1). For comparison of the different crystallization experiments, these crystals were always resuspended for 90 s until the suspension was pumped to the slug formation.

For quantifying the effect of operating parameters on the PSD and product yield, the volume flow rate, the liquid hold up and the cooling rate were varied (see Section 3.3). For that, the tubing length was varied from $L_{tubing} = 13.25$–26.5 m so that under all experimental conditions the peristaltic pump was able to overcome the pressure drop along the tubing's length (up to $\Delta p_{drop} = 1$ bar). These tubing lengths used are compara-

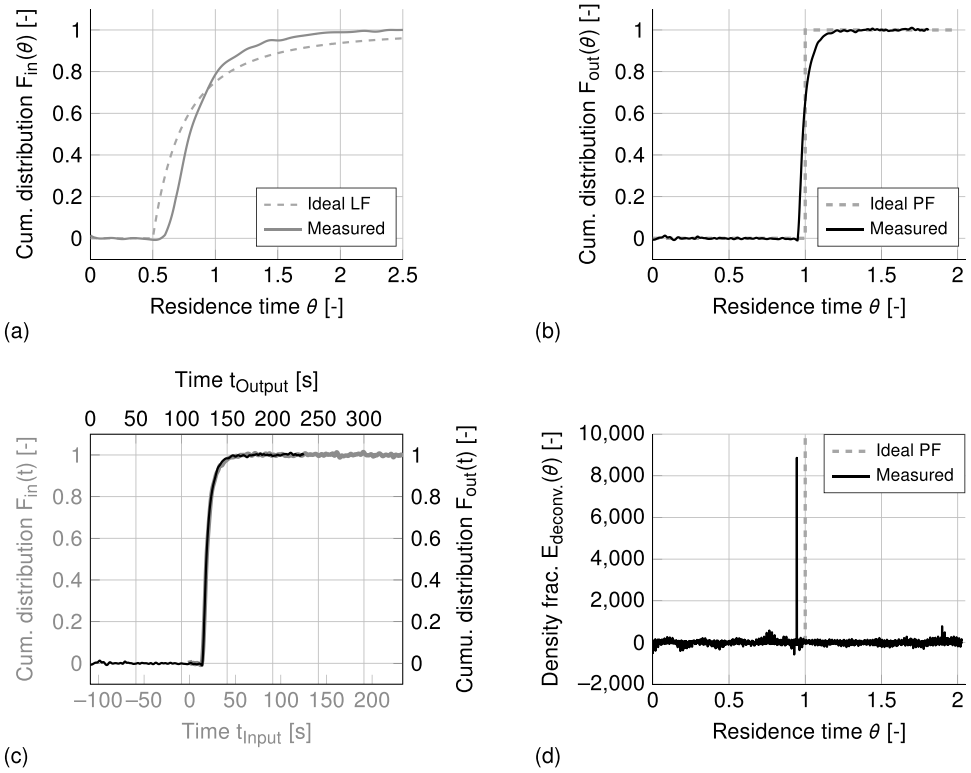

Fig. 2 – Distribution functions of the liquid phase for (a) the inlet of the slug flow zone representing the behavior of the periphery and the ideal curve of a laminar flow (LF). The volume flow rate inside the periphery was equal to $Q_{Liq} = 10\,mL\,min^{-1}$ leading to a residence time of $\tau = 23\,s$. (b) the outlet of the apparatus including the periphery as well as the slug flow zone and the ideal curve of a plug flow (PF). Operating parameters were set to $Q_{tot} = 30\,mL\,min^{-1}$ and $\epsilon_{L,0} = 0.33$ leading to a residence time of $\tau = 129\,s$. (c) inlet (gray) and outlet (black), whereby the signals are depicted over their time measured. A shift of the signals leading to an overlap shows the same curvature proving plug flow behavior. Operating conditions were equal to the ones of (b). (d) The slug flow zone only. By deconvolution of the input and output signal of (c) the exit age distribution is obtained. Operating conditions were equal to the ones of (b) leading to a residence time of $\tau = 115\,s$ inside the slug flow zone only.

ble to the ones used in literature (Eder et al., 2012; Besenhard et al., 2017; Mou and Jiang, 2020). Furthermore, depending upon the operating conditions investigated the slugs were cooled down from $\vartheta = 50\,°C$ to different end temperatures (see Section 3.3).

For the quantification of the PSD and its subpopulations of single crystals and non-single crystals (aggregates/agglomerates), slugs at the SFC's end were collected in saturated solution inside a tempered vessel equipped with an overhead stirrer ($V = 1\,L$, $n = 250\,rpm$, $\vartheta^* = 30\,°C$). After a sampling time of approx. 90 s to ensure at least 2000 crystals collected, the PSD was measured by means of the imaging sensor QICPIC and the wet dispersion system LIXELL (Sympatec company). For image acquisition and further analysis via Matlab using artificial neural networks, the reader is referred to literature (Heisel et al., 2018, 2019a,b).

The relative yield obtained was determined with the help of the solute's concentration gravimetrically measured at the feed suspension vessel and at the SFC's outlet (4 samples for each measurement point). For that, a suspension's volume of at least $V = 8\,mL$ per sample was collected and filtered with the help of a tempered syringe filter (Macherey-Nagel GmbH&Co.KG, Chromafil Xtra PTFE, pore size 0.45 µm). The filtrates were dried for 48 h at 50 °C in a vacuum oven. By Eq. (10), the relative yield Y_{rel} was calculated using the saturation concentration from the feed suspension tank $c^*(\vartheta_0)$, the experimentally determined concentration $c(\vartheta_{end})$ and its respective theoretical saturation concentration $c^*(\vartheta_{end})$.

$$Y_{rel} = \frac{c^*(\vartheta_0) - c(\vartheta_{end})}{c^*(\vartheta_0) - c^*(\vartheta_{end})} \tag{10}$$

3. Results and discussion

3.1. *Residence time distribution of liquid and solid phase*

Fig. 2 shows the results of the liquid phase's RTD_L for operating conditions of $Q_{tot} = 30\,mL\,min^{-1}$ and $\epsilon_{L,0} = 0.33$. Comparing the signal at the slug flow zone's inlet with the one of an ideal laminar flow, it becomes visible that they are almost equal (see Fig. 2(a)). This agreement was not surprising as a Reynolds number of Re = 70 inside the periphery already led to the conclusion of laminar flow behavior. The slight deviations from the ideal course can be explained with the flow conditions inside the peristaltic pump through which the solution is pumped to the slug formation zone.

From the visual observation of the slug flow, no wall film was recognizable, and slugs as well as the gaseous phase showed a square shape (exemplary video can be found in Supporting Information), proving that back mixing between adjacent slugs could be avoided which is also seen in the steep

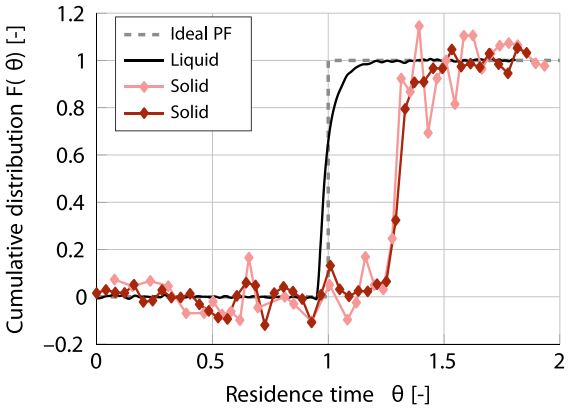

Fig. 3 – Cumulative residence time distribution of liquid and solid phase, whereby the RTD_S was measured twice (both separately shown). Operating conditions were set to $\dot{Q}_{tot} = 30\,mL\,min^{-1}$ and $\epsilon_{L,0} = 0.33$ ($\tau = 129\,s$). For the measurement of the solid phase, the solid content was chosen to $w_{Solid} = 5.1\,wt.\text{-}\%$ and the median particle size to $d_{50,3} = 300\,\mu m$. (For interpretation of the references to color in the text, the reader is referred to the web version of this article.)

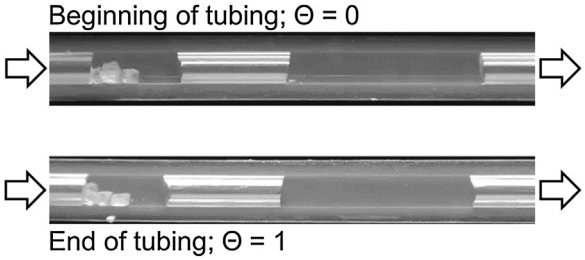

Fig. 4 – Images of the beginning (top) and end (bottom) of the slug flow zone, while crystals with a maximum size of $d_{Feret} = 2.5\,mm$ were transported inside one single slug. The same crystals seen at the beginning of the slug flow zone leave the slug flow zone after $t = 7.4\,min$.

increase of the RTD at a normalized residence time of $\theta = 1$ indicating plug flow behavior (see Fig. 2(b)). However, whether the RTD of ideal plug flow inside SFC is obtained, can only be proven by deconvolution of the input and output signal. By shifting the signals measured over time of SFC's in- and outlet towards each other (see Fig. 2(c)), a first impression becomes visible: Since there is no difference in the course of the two functions detectable, the particular inlet signal leaves the SFC in the same manner except for a time delay. By deconvolution of the signal making use of Fast Fourier transform (see Eq. (9)), a steep peak in the E curve, comparable to the one of ideal plug flow, becomes clear (see Fig. 2(d)). However, the peak arises before $\theta = 1$ meaning that the volume elements leave the apparatus slightly before passing one hydrodynamic residence time ($\bar{t} = 109\,s$, $\tau_{SF,L=7\,m} = 115\,s$). Due to the pressure drop over the SFC's tubing length ($\Delta p_{drop} = 0.19\,bar$), the compressible gaseous phase expands, leading to an increased flow velocity and hence, a residence time, which is slightly lower than the ideal one.

With the Bodenstein number the degree of axial dispersion can be quantitatively described. For Bodenstein numbers higher than 100, plug flow behavior is assumed. For all the operating parameters investigated in this study ($\dot{Q}_{tot} = 30$–$60\,mL\,min^{-1}$ and $\epsilon_{L,0} = 0.33$–0.66), Bodenstein numbers in the range from 792 up to 1323 for the whole plant including periphery and slug flow zone were calculated (see Table S1 in Supporting Information). Hence, it can be concluded that for the liquid phase an ideal plug flow behavior inside the slug flow zone was obtained independently from the operating conditions investigated.

The result of the RTD_S is presented in Fig. 3, measured for operating conditions of $\dot{Q}_{tot} = 30\,mL\,min^{-1}$ and $\epsilon_{L,0} = 0.33$ to be comparable to the ones of the liquid phase measurement.

Thereby, it has to be kept in mind that the samples for gravimetrical measurements are taken at the SFC's end so that the RTD_S includes the periphery and slug flow zone. From the red/dark curve, representing the solid phase, a time shift of 40 s between RTD_L and RTD_S is detectable. This time shift is caused by slower transportation of the solid phase than the liquid phase through the periphery. In order to form the slug flow inside the T-junction, the crystals need to be pumped through the periphery, which was arranged as vertical as possible. Still, crystals tended to roll down the periphery resulting in a longer time to reach the slug formation zone compared to the liquid phase. Experimentally, a time difference of 44 s could be measured, which is in good agreement with the time shift determined from the RTD_S (see Fig. 3). Next, fluctuations and negative values for the RTD_S can be observed. These originate from the measurement of the solid content with a gravimetrical approach. Due to the small sample volume taken manually ($V \approx 0.9\,mL$), small deviations in mass after drying can have a significant effect on the solid content's measurement and thus, on the RTD_S. Nevertheless, overall a clear increase in both the F curves of the RTD_S is detectable, showing the successful measurement. Comparing the curvatures of the RTD_L and RTD_S with each other, it can be observed that they are equal. Hence, the same width of distribution is registered, leading to the conclusion that also for the RTD_S ideal plug flow behavior is obtained. Thereby, it should be emphasized that these results can only be obtained as long as a wall film of the liquid phase is avoided and when especially big crystals do not break the interface of gaseous and liquid phase.

To confirm the latter statement, extreme operating conditions (large crystals, low flow rate, high liquid holdup) were examined. However, by increasing the crystal size, the pump was blocked. Hence, the impact of crystal size was evaluated by directly adding crystals into the T-junction. L-alanine crystals up to a maximum Feret diameter of approx. $d_{Feret} = 2.5\,mm$ were injected. In order to even trigger the crystals to leave the slug by breaking through the interfacial area, operating conditions minimizing the internal circulations were used ($\dot{Q}_{tot} = 7\,mL\,min^{-1}$ and $\epsilon_{L,0} = 0.66$). From Fig. 4 it is observable that the exact same three crystals entering the slug flow zone (upper picture) also leave the apparatus after one residence time (bottom picture). Hence, independent of the crystal size, a narrow RTD_S for the SFC was successfully proven.

However, this might not be transferable to other SFCs. Besenhard et al. (2017) showed in their studies that in the presence of a wall film crystals smaller than this film are trapped within it, resulting in a broader RTD_S, which is even more broadened in their studies for higher volume flow rates. However, as long as a stable slug flow without a wall film of the liquid phase is present, this study showed that a plug-flow-like RTD for the liquid as well as the solid phase for all the operating conditions investigated is obtained. Hence, regarding the crystallization experiments, the impact of operating parameters on the RTDs is negligible.

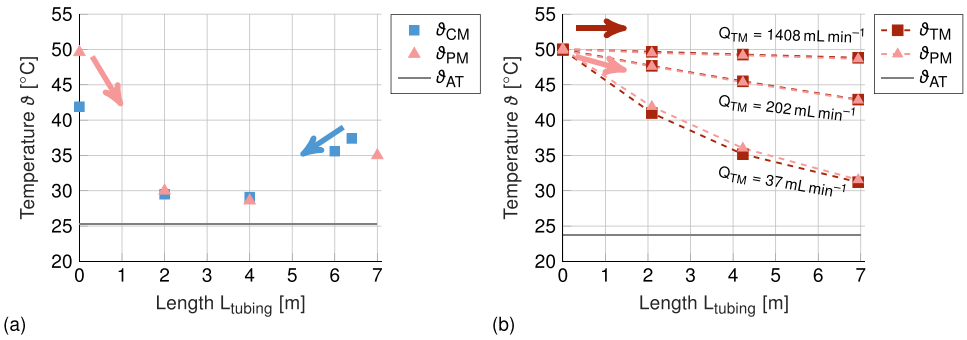

Fig. 5 – Steady state temperature profiles for (a) counter current flow of process and cooling medium over the length of tubing. The ambient temperature (AT) is represented by the gray line. The slug flow was operated at $Q_{tot} = 20\,mL\,min^{-1}$ and $\epsilon_{L,0} = 0.5$, while the volume flow rate of cooling medium was set to $Q_{CM} = 10\,mL\,min^{-1}$. (b) Insulating co-current flow of process and tempering medium over the length of tubing. Different volume flow rates of tempering medium are depicted leading to different temperatures at the end of slug flow zone. The dashed lines serve for better visualization only. The ambient temperature is represented by the gray line. Operating conditions for slug flow were set to $Q_{tot} = 20\,mL\,min^{-1}$ and $\epsilon_{L,0} = 0.5$.

Nevertheless, the residence time itself should be increased in order to provide enough time for crystal growth which is usually a slow process. Next to an extension of the tubing, the operating parameters can be chosen in a way such that this time is increased. Despite the fact that the suspension inside slugs is reduced, the volume flow rate is set to $Q_{tot} = 20\,mL\,min^{-1}$ for further experiments to increase the residence time.

3.2. *Cooling strategy*

To avoid the use of multiple water baths for cooling of a tubular crystallizer, as mentioned in Section 1, a counter current flow heat exchange concept was chosen in this study, first. The proof of concept is evaluated with the help of the prototype SFC characterized by a short tubing length used ($L_{tubing} = 7\,m$). With the aim of cooling from 50 to 25 °C along the entire tubing's length, a cooling from 50 to 40 °C is pursued first for reduced tubing length. Hence, from the end of SFC's tubing the cooling medium (CM) flows with a temperature of 40 °C and the process medium (PM) enters the tubing with a temperature of 50 °C, indicated by the arrows in Fig. 5(a). After reaching steady state in slug flow and the temperatures of PM and CM, the inlet and outlet's temperatures were measured at full length to not disturb the slug flow regime. For measurement of intermediate temperatures, the tubing's intersections were successively opened from SFC's end to its beginning. Fig. 5(a) shows the respective temperature profile for the counter current heat exchange operated with $Q_{tot} = 20\,mL\,min^{-1}$ and $\epsilon_{L,0} = 0.5$. Regarding the course of PM's temperature, a steep decrease directly within a length of 2 m down to a temperature of 30 °C is detectable. Furthermore, also the CM's temperature hits the same value at this particular tubing length. This was not expected as the CM's temperature in counter current flow was set to a higher value ($\vartheta_{CM,end} = 40\,°C$). However, when having a look at the ambient temperature of 25 °C, the progress of the temperature curve can be explained with heat losses to the environment. From the heat balance (see Supporting Information) a CM's flow rate of $Q_{CM} = 10\,mL\,min^{-1}$ was calculated and hence, adjusted leading to flow rates in the outer tubing of $v_{CM} = 1.75\,mm\,s^{-1}$. The respective low heat transfer to the CM in combination with the high heat transfer area leads to a significant impact of heat losses to the environment ($\vartheta_{AT} = 25.3\,°C$), although the outer tubing was insulated with polyethylene (PE) tubing. Hence, temperatures in the middle of the slug flow zone beneath CM's and PM's temperature result.

Therefore, the idea came up to use this high degree of heat exchange with the environment on purpose while maintaining the benefits of the tube-in-tube construction: The SFC is cooled down in co-current mode, but the inlet temperature of the tempering medium (TM) is set equal to the one of the PM's inlet temperature. In this way, cooling can be achieved via heat loss, and the TM acts as active insulation. Hence, for higher volume flow rates of TM a smaller temperature decrease is expected, while higher cooling rates are obtained for lower TM flow rates.

The results for the steady state temperature profiles are shown in Fig. 5(b) for operating conditions of $Q_{tot} = 20\,mL\,min^{-1}$ and $\epsilon_{L,0} = 0.5$. Hereby, it has to be noted that the PM as well as the TM flow in the same direction from the slug formation to the slug flow's tubing end. In contrast to the temperature profile of counter-current heat exchange (see Fig. 5(a)), a smooth decrease of temperature from 50 °C to its respective end temperature is discernible. Thereby, the dashed lines are added to enhance the temperature profiles' visualization and do not represent the actual course between the measurement points.

Different cooling rates are adjustable by changing the outlet temperature with the help of varied TM volume flow rate. Moreover, the PM temperature course follows the one of the superimposed TM. As expected, the superior heat transfer of the slug flow regime leads to the fact that the temperatures of TM and PM equal each other. Especially for the temperature course of a crystallization process, this behavior is greatly beneficial. By measuring the TM temperature course, the progress of PM temperature is known. Therefore, the disturbance of the slug flow via implementation of a probe is avoided. Overall, it can be concluded that with the insulating co-current heat exchange, a smooth cooling of the SFC is successfully implemented.

In the next step, the applicability for a longer tubing length is needed in order to increase the residence time inside the SFC. Exemplary, the temperature profile for a cooling from 50 to 25 °C for a tubing length of $L_{tubing} = 33.4\,m$ is shown in Fig. 6.

Again, the results show a smooth decline of temperature over the entire length of the crystallizer by using one thermostat only. With respect to its curvature, a degressive profile

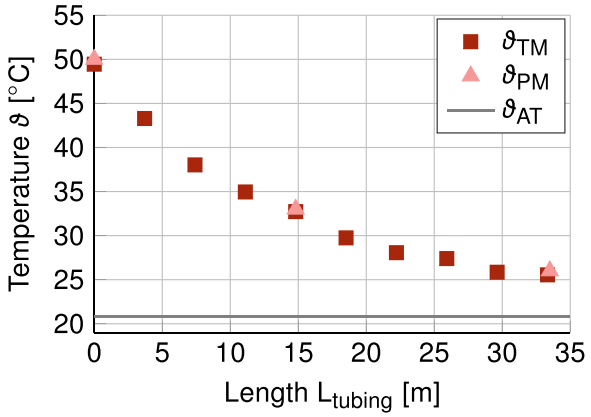

Fig. 6 – Exemplary steady state temperature profile for insulating co-current concept at total tubing length of $L_{tubing} = 33.4$ m. The ambient temperature is depicted in gray. Operating conditions for the slug flow were set to $Q_{tot} = 20\,mL\,min^{-1}$ and $\epsilon_{L,0} = 0.5$, the volume flow rate of tempering medium was equal to $Q_{tot} = 111\,mL\,min^{-1}$.

is observable, meaning that the cooling rate decreases over the tubing length. Hence, for crystallization experiments an increased supersaturation at the tubing's beginning must be kept in mind. With this knowledge special focus should be set to the cooling at the tubing's beginning for chemical systems showing small nucleation thresholds as supersaturation peaks might arise. However, compared to the use of water baths, the concept of insulated co-current heat exchange reduces the amount of thermostats needed combined with a smooth cooling over the tubing's length.

3.3. *Effect of operating parameters on product quality*

An enhanced suspension, which might lead to less agglomeration and improved control of PSD, is influenced by the slug flow zone's operating parameters. Hence, by quantifying their effect on the PSD and its subpopulations, knowledge about enhanced product quality control might be generated. Operating parameters like total volume flow rate Q_{tot} influencing the slugs' velocity and the liquid hold up $\epsilon_{L,0}$ manipulating the slug length showed in previous experiments significant impact on the goodness of suspension. Thus, these represent decisive parameters for an enhanced control of crystalline product quality. Next to that, the average cooling rate $\bar{\kappa} = \frac{T_0 - T_{end}}{\tau}$ determining the supersaturation is an important factor to keep in mind. Thereby, T_0 represents the temperature at slug formation and T_{end} the SFC's outlet temperature. Previous experiments showed that average cooling rates of $\bar{\kappa} = 1.8\,K\,min^{-1}$ avoid secondary nucleation (see Supporting Information Fig. S8).

It should be emphasized that the SFC's operating parameters are coupled such that an independent investigation of each parameter on the crystalline product quality becomes challenging: For a constant tubing length, an increased Q_{tot} leads to a decreased residence time which might result in less crystal growth, but also to an enhanced suspension inside the slugs (Termühlen et al., 2019). In addition to that, an increased flow rate also increases the average cooling rate, since the residence time is decreased ($\bar{\kappa} = \frac{T_0 - T_{end}}{\tau}$). Hence, suspension, cooling rate, and residence time are coupled with each other, when varying Q_{tot} while keeping all other design and operating parameters constant.

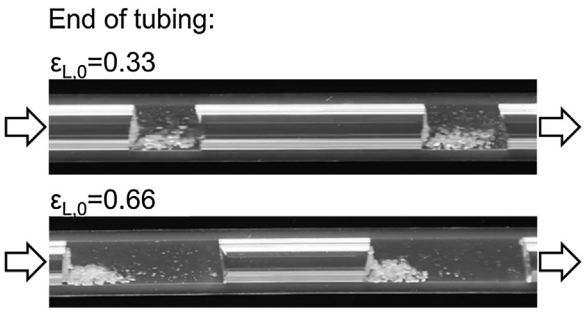

Fig. 7 – Image of slug flow at the end of the tubing for a liquid hold up of $\epsilon_{L,0} = 0.33$ (top) and $\epsilon_{L,0} = 0.66$ (bottom). Seeded crystallization was operated with $Q_{tot} = 20\,mL\,min^{-1}$ and cooled down from 50 °C to approx. 31 °C.

Only the liquid hold up manipulating the slug length can be altered without changing residence time or cooling rate so that it is investigated first (see Section 3.3.1 and Table 1).

For decoupling the parameters Q_{tot} and $\bar{\kappa}$, the residence time should be kept constant while increasing the total volume flow rate. Next to the slugs' velocity, the tubing length determines the residence time. The length can be varied for different Q_{tot} to guarantee the same residence time.

In a next step, the effect of increased cooling rate is investigated. For that, the total volume flow rate Q_{tot} is varied only while keeping the tubing length as well as the temperatures at slug formation and outlet constant to achieve an equal theoretical yield. Thus, the residence time is decreased while the average cooling rate $\bar{\kappa}$ is increased (see Table 1). The hypothesis whether an increased cooling rate might overcome a limiting residence time can be proven (see Section 3.3.3).

All experimental data measured can be found in Supporting Information in Table S2.

3.3.1. *Effect of liquid hold up $\epsilon_{L,0}$*

By manipulating the liquid hold up $\epsilon_{L,0}$, the slug lengths are varied, as can be seen in the images taken at SFC's end in Fig. 7. At first sight, it becomes clear that the crystals are more distributed for smaller slugs ($\epsilon_{L,0} = 0.33$). However, at the gas-liquid interphase, crystals still slightly cluster. For the longer slug length, this phenomenon is even intensified, which might enhance agglomeration. The quantitative effect of the slug length on the PSD and its subpopulations can be found in Fig. 8. The PSD and also its subpopulations are significantly shifted towards bigger crystal sizes for both liquid hold ups. Hence, in all experiments, conducted three times each, reproducible crystal growth is observable. In accordance with the results of Su and Gao (2018), the PSD is significantly shifted towards bigger product crystal sizes for longer slugs compared to the one for smaller slugs (see Fig. 8(a)). However, as mentioned in the introduction, this has to be investigated in detail with the help of the distribution of single crystals (sc) and aggregated/agglomerated crystals (ag) (see Fig. 8(b)). Comparing the seed and product single crystals only, less single crystals are detected for both slug lengths after crystallization. In between the single crystal distribution of the different slug lengths, there is no significant difference. When comparing the aggregated/agglomerated product crystals only, the ones produced in longer slugs are significantly bigger than those from smaller slugs. Furthermore, their width of distribution is broader compared to the agglomerates' distribution of the small slugs. As less suspension in longer slugs leads to higher contact times between the specific crystals, agglomeration is favored.

Table 1 – Design and operating parameters chosen for the determination of their effect on the product quality ($d_{i,tubing} = 3.18$ mm).

	Q_{tot} [mL min^{-1}]	$\epsilon_{L,0}$ [–]	τ [min]	L_{tubing} [m]	$\bar{\kappa}$ [K min^{-1}]	ϑ_0 °C	ϑ_{end} °C
Effect of $\epsilon_{L,0}$	20	**0.33**	10.5	26.5	1.8	50	31
	20	**0.66**	10.5	26.5	1.8	50	31
Effect of Q_{tot}	**20**	0.5	5.25	**13.25**	1.8	50	40.5
	40	0.5	5.25	**26.5**	1.8	50	40.5
Effect of $\bar{\kappa}$	**20**	0.5	**10.5**	26.5	**1.8**	50	31
	40	0.5	**5.25**	26.5	**3.6**	50	31

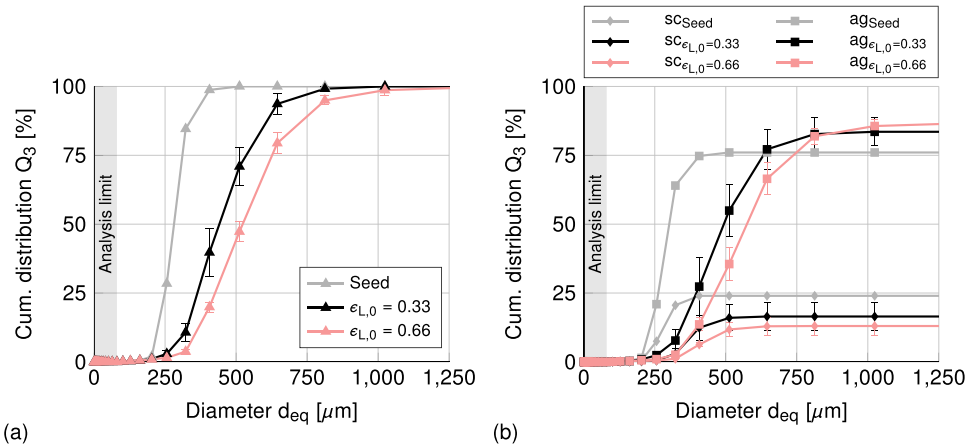

Fig. 8 – Volume based cumulative size distribution of (a) seed (gray, $n_{part,tot} = 2207$) and product particles for a liquid hold up of $\epsilon_{L,0} = 0.33$ (black, $n_{part,tot} = 7984$) and $\epsilon_{L,0} = 0.66$ (pink/light, $n_{part,tot} = 9058$). (b) Single and aggregated/agglomerated seed (gray) and product crystals for a liquid hold up of $\epsilon_{L,0} = 0.33$ (black) and $\epsilon_{L,0} = 0.66$ (pink/light). The SFC ($L_{tubing} = 26.5$ m) was operated with $Q_{tot} = 20$ mL min^{-1} and cooled from 50 °C to 31 °C. (For interpretation of the references to color in this figure legend, the reader is referred to the web version of this article.)

Since the residence time of $\tau = 10.5$ min and the cooling from 50 °C to 31 °C is equal for both liquid hold ups investigated, no difference in yield is observable. In both cases the relative yields of $Y_{rel,\epsilon_{L,0}=0.33} = 82.7 \pm 6.6\%$ and $Y_{rel,\epsilon_{L,0}=0.66} = 77.7 \pm 4.0\%$ do not significantly differ from each other (see Fig. S6 in Supporting Information).

In combination with the PSD and its subpopulations it is still surprising that with shorter slugs smaller crystals with a narrower distribution's width are obtained under the same yield. This can be explained with the suspension behavior as well. As in shorter slugs the crystals are horizontally more spread, the contact times between crystals are reduced leading to smaller agglomerates as the PSD's subpopulations show (see Figs. 7 and 8).

However, it also has to be kept in mind that with shorter slugs space-time yield is decreased as the tubing contains a higher fraction of gaseous phase for a liquid hold up of $\epsilon_{L,0} = 0.33$. Therefore, regarding the liquid hold up and its effect on the product quality in terms of PSD and agglomeration, smaller slugs are beneficial for a narrower PSD. However, as smaller slugs decrease the space-time yield, a compromise of $\epsilon_{L,0} = 0.5$ is suggested and used for further experiments.

3.3.2. *Effect of total volume flow rate Q_{tot}*

The suspension behavior inside slugs can be even more affected by increasing the flow velocity. As seen before, this can narrow the PSD. Hence, the total volume flow rate is doubled (from $Q_{tot} = 20$ mL min^{-1} to $Q_{tot} = 40$ mL min^{-1}) to not shorten the residence time too much ($\tau_{40\,mL\,min^{-1},\,L=26.5\,m} = 5.25$ min).

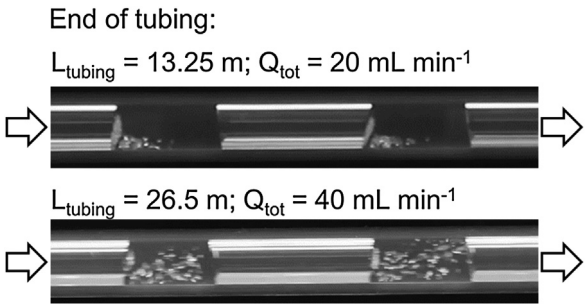

Fig. 9 – Image of slug flow at the end of tubing for a total volume flow rate and tubing length of $Q_{tot} = 20$ mL min^{-1} and $L_{tubing} = 13.25$ m (top) and $Q_{tot} = 40$ mL min^{-1} $L_{tubing} = 26.5$ m (bottom). Seeded crystallization was operated with $\epsilon_{L,0} = 0.5$ and cooled down from 50 °C to 40.5 °C.

In Section 3.3, the interaction of the effects total volume flow rate, suspension behavior, residence time, and cooling rate was already explained. Thus, to investigate the effect of total volume flow rate Q_{tot}, the tubing needs to be shortened by half for a low value of Q_{tot} to guarantee the same residence time for the high value of Q_{tot}. With respect to the SFC's end temperature, the average cooling rate from the experiments previously performed ($\bar{\kappa} = 1.8$ K min^{-1}) was kept constant resulting in a cooling from 50 °C to 40.5 °C.

From the images taken at the tubing's outlet, a significant difference in the suspension behavior is observable in Fig. 9. Compared to the upper image, the higher flow velocity leads to an improved suspension in the horizontal as well

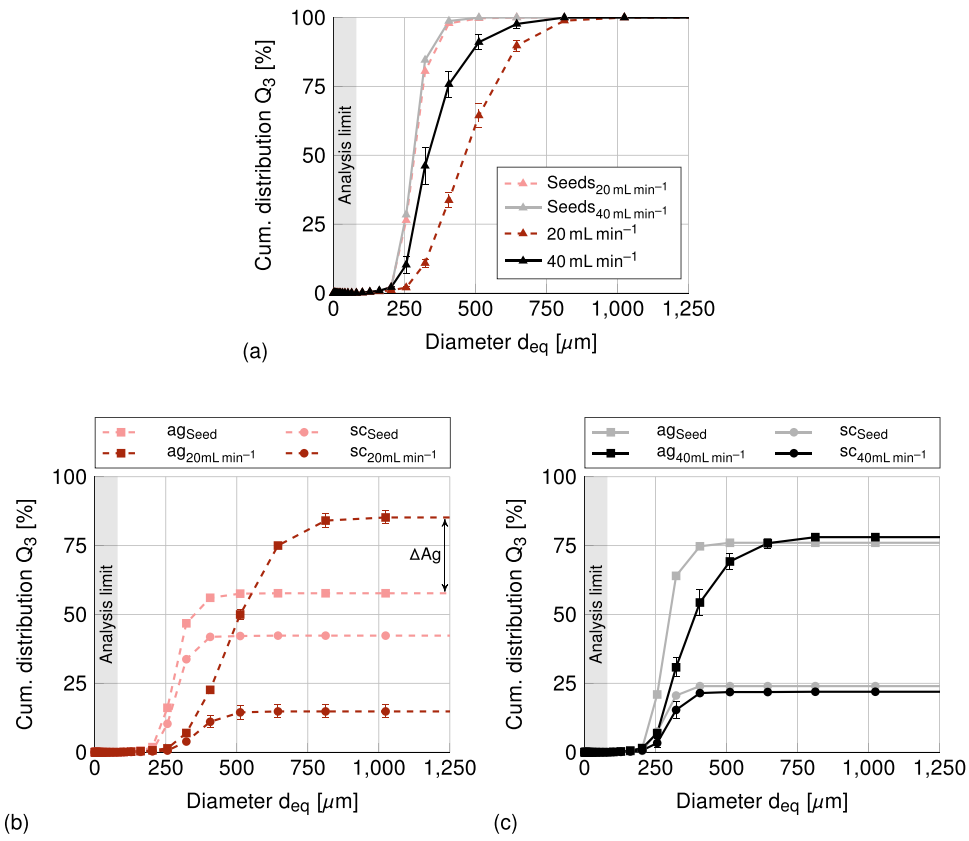

Fig. 10 – Volume based cumulative size distribution of (a) seed (gray/solid, $n_{part,tot} = 2207$ and pink/dashed) and product particles for a total volume flow rate of $Q_{tot} = 20\,mL\,min^{-1}$ (red/dark dashed, $n_{part,tot} = 5356$) and $Q_{tot} = 40\,mL\,min^{-1}$ (black/dark solid, $n_{part,tot} = 5196$). (b) Single and aggregated/agglomerated seed (pink dashed) and product crystals for a total volume flow rate of $Q_{tot} = 20\,mL\,min^{-1}$ (red/dark dashed). (c) Single and aggregated/agglomerated seed (gray/ light) and product crystals for a total volume flow rate of $Q_{tot} = 40\,mL\,min^{-1}$ (black/dark). The SFC cooled from 50 °C to 40.5 °C. (For interpretation of the references to color in this figure legend, the reader is referred to the web version of this article.)

as the vertical direction in the bottom image. This prevents accumulation in the rear end corner so that crystals' clustering at the interphase between slug and bubble is minimized. Quantitatively, this effect also impacts the PSD and its subpopulations (see Fig. 10). Comparing the seed crystals with the product crystals in Fig. 10(a), a shift towards bigger crystals is seen for both flow rates investigated. However, smaller crystals with a narrower distribution's width are detected for the high total volume flow rate. The broadened width of distribution for the low total volume flow rate can be explained with increased agglomeration as the PSD contains 85% of aggregates/agglomerates (see Fig. 10(b)). Thereby, in Fig. 10(c) the distribution of aggregation/agglomerates ends in a value of 78%. It has to be noted that different seed crystals were used for these experiments. Although the seed crystals showed equal PSDs, as seen in Fig. 10(a), the amount of agglomerates showed significant differences ($Ag_{Seed,20\,mL\,min^{-1}} = 58\%$, $Ag_{Seed,40\,mL\,min^{-1}} = 76\%$). Nevertheless, the difference in the respective agglomeration degrees $\Delta Ag = Ag_{Prod} - Ag_{Seed}$ is significant: For high total volume flow rates the increase in ΔAg amounts only 2% whilst for the low flow rate the agglomeration degree is inclined by $\Delta Ag = 27\%$. Thus, it can be concluded that though using more agglomerated seed crystals, a higher total volume flow rate resulting in improved suspension leads to less agglomeration of the product crystals.

Hence, for an SFC's operation with respect to obtaining a narrow PSD with a reduced degree of agglomeration, a high total volume flow rate leading to improved suspension is beneficial. However, along with that, the residence time is decreased and cannot be easily extended as the tubing length is limited by the maximum pressure drop the pump has to overcome. This might lead to smaller product crystals. As the supersaturation is the main factor for crystal growth (Ostermann et al., 2018), the cooling rate is one parameter that could further increase crystal size while maintaining a narrow PSD with a low amount of agglomerates.

3.3.3. *Effect of cooling rate $\bar{\kappa}$ under varying residence time*

For all the experiments conducted with an average cooling rate of $\bar{\kappa} = 1.8\,K\,min^{-1}$, the SFC could be operated without observing any wall crystallization. Hence, the operating limit was not reached why the cooling rate was further increased. Two different volume flow rates of $Q_{tot} = 20\,mL\,min^{-1}$ and $Q_{tot} = 40\,mL\,min^{-1}$ were compared again, while keeping all other parameters constant ($\epsilon_{L,0} = 0.5$, $L_{tubing} = 26.5\,m$). Hence, for a high volume flow rate ($Q_{tot} = 40\,mL\,min^{-1}$), the suspension is improved, and a higher average cooling rate $\bar{\kappa} = 3.6\,K\,min^{-1}$ is obtained within a decreased residence time ($\tau_{L=26.5\,m} = 5.25\,min$, cooling from 50 °C to 31 °C).

This decreased residence time's effect becomes obvious in the relative yields achieved: While for the lower flow rate implying a residence time of 10.5 min a relative yield of $Y_{rel} = 76.9 \pm 1.1\%$ is obtained, the supersaturation can only be degraded to a yield of $Y_{rel} = 59.9 \pm 3.7\%$ for the shorter residence time (see Fig. S7 in Supporting Information).

A significant shift of the PSDs towards bigger crystals is seen for both volume flow rates investigated (see Fig. 11(a)). When focusing on a narrow PSD and minimizing the agglom-

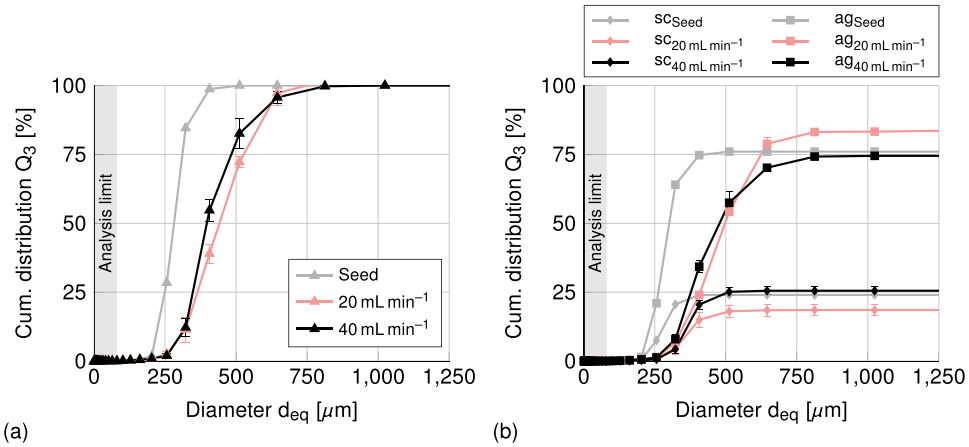

Fig. 11 – Volume based cumulative size distribution of (a) seed (gray) and product particles for a total volume flow rate of $Q_{tot} = 20\,mL\,min^{-1}$ (pink, $n_{cryst,tot} = 7822$) and $Q_{tot} = 40\,mL\,min^{-1}$ (black, $n_{cryst,tot} = 9619$). (b) Single and aggregated/agglomerated seed (gray) and product crystals for a total volume flow rate of $Q_{tot} = 20\,mL\,min^{-1}$ (pink) and for a total volume flow rate of $Q_{tot} = 40\,mL\,min^{-1}$ (black). The SFC was cooled from 50 °C to 31 °C and the tubing length amounted 26.5 m. (For interpretation of the references to color in this figure legend, the reader is referred to the web version of this article.)

eration degree, a higher volume flow rate under remaining constant conditions is more beneficial (see Fig. 11). The higher total volume flow rate (black/dark curve) shows a narrower distribution's width. This can be explained with less agglomeration analyzing the distributions of aggregates/agglomerates in detail (see Fig. 11(b)). Although for higher volume flow rate a higher supersaturation inside slug flow is present due to the higher cooling rate, fewer agglomerates are formed. This was not expected as an increased supersaturation does not only affect crystal growth but also the agglomeration kinetics. However, the improved suspension due to the higher flow rate has an opposite effect on agglomeration. As the courses of seed and product distribution of agglomerates end in the same value of approx. 75%, it can be concluded that there is no effect on agglomeration. This is in contrast to the small volume flow rate used as the curve of distribution of product agglomerates clearly exceeds the one for the seed crystals in the end value. Furthermore, the width of distribution is broadened from $d_{90-10,ag,3} = 137\,\mu m$ for the seed crystals to $d_{90-10,ag,3} = 364\,\mu m$ for the agglomerated product crystals.

By having a look on the single crystals only, it can be concluded that using a higher volume flow rate under cooling from 50 °C to 31 °C shifts the course of the distribution of single crystals by approximately 90 μm without significantly changing its width.

A decrease in residence time due to higher flow rates is overcome by stronger cooling such that not only the product quality in terms of agglomeration can be maintained, but crystal growth is also promoted. Median particle sizes of $d_{50,3} = 397\,\mu m$ for the high volume flow rate ($\tau = 5.25$ min) are obtained being comparable to the ones for the small volume flow rate of $d_{50,3} = 441\,\mu m$ ($\tau = 10.5$ min).

4. Summary and conclusion

The aim of this contribution was to design and operate a continuous slug flow crystallizer with focus on a narrow PSD, minimized agglomeration, and enhanced process yield. Remembering the five requirements from the introduction it was shown that a stable convex shaped slug flow results in a plug-flow-like RTD for the liquid as well as the solid phase independent of the operating conditions investigated. The insulated co-current tube-in-tube heat exchange enabled smooth cooling using one thermostat only over the entire slug flow zone. Along with that, we showed that the process medium's temperature was always equal to the one of the surrounding tempering medium due to the high SFC's heat transfer rates. In contrast to the use of (multiple) water baths – commonly used in literature – supersaturation peaks could be avoided.

By making use of seeding, the median particle size was shifted by 240 μm after a residence time of 10.5 min only ($Q_{tot} = 20\,mL\,min^{-1}$, $\epsilon_{L,0} = 0.66$). Although the residence time itself was rather low, compared to e.g., batch processes, a high process yield ($Y_{rel} = 82.7 \pm 6.6\%$) and a significant crystal growth were detectable originating from high supersaturations whilst still avoiding secondary nucleation. Moreover, a high reproducibility of the product's PSD ($d_{50,3} = 523 \pm 14\,\mu m$, $d_{90-10,3} = 402 \pm 24\,\mu m$) was observed. However, a broadened distribution's width was detected. With the help of the PSD's subpopulations of single crystals and non-single crystals (aggregates/agglomerates) this phenomenon was traced back to increased agglomeration of the product crystals. Regarding the RTD and the PSD obtained after crystallization, it can be concluded that a narrow RTD of an apparatus does not automatically lead to a narrow PSD. Of course, a well designed apparatus is a prerequisite for obtaining a narrow PSD, but the suspension behavior manipulable by the operating parameters also plays a key role as it determines the contact time between particles.

Making use of low flow rates, leading to less suspension inside slugs and even a clustering at the slug/bubble interphase, demonstrated that high contact times between particles result in a high agglomeration degree. By increasing the volume flow rate and thus, improving the suspension we showed that agglomeration inside the growth zone was successfully avoided and the PSD was shifted towards bigger crystals without broadening its width. Thereby, it has to be kept in mind that the product's quality is of course highly dependent upon the seed's quality.

After a short start up phase of only one residence time due to the apparatus' plug-flow-like RTD, the continuous operation

could be maintained for about 40 min as the feed suspension vessel (V = 450 mL) was only filled once to guarantee a constant solid content. Hence, an in-situ seed generation is essential for a long time continuous operation. Though no fouling or blocking was observed during the experiments in this study, for long time operation the challenge of encrustations has to be reevaluated again.

It has to be kept in mind that these achievements hold for the substance system L-alanine/water being characterized by rather fast growth kinetics as the residence time is limited in the SFC designed in this work. Hence, in future works, this residence time should be extended to allow crystallization of various substance systems. Nevertheless, the SFC's design in this study seems to be promising as with its particular residence time increased crystal growth with enhanced focus on product quality control could be achieved. Hence, a deeper understanding towards continuous crystallization of fine chemical was gained.

Conflicts of interest

None declared.

Appendix A. Supplementary data

Supplementary data associated with this article can be found, in the online version, at https://doi.org/10.1016/j.cherd.2021.04.006.

Declaration of Competing Interest

The authors report no declarations of interest.

References

Alvarez, A.J., Myerson, A.S., 2010. Continuous plug flow crystallization of pharmaceutical compounds. Cryst. Growth Des. 10, 2219–2228.

Alvarez, A.J., Singh, A., Myerson, A.S., 2011. Crystallization of cyclosporine in a multistage continuous MSMPR crystallizer. Cryst. Growth Des. 11, 4392–4400.

Baerns, M., 2013. Technische Chemie, 2nd ed. Wiley, Hoboken.

Beckmann, W., 2013. Crystallization: Basic Concepts and Industrial Applications. Wiley-VCH, Weinheim.

Besenhard, M.O., Neugebauer, P., Scheibelhofer, O., Khinast, J.G., 2017. Crystal engineering in continuous plug-flow crystallizers. Cryst. Growth Des. 17, 6432–6444.

Briggs, N.E.B., Schacht, U., Raval, V., McGlone, T., Sefcik, J., Florence, A.J., 2015. Seeded crystallization of beta-l-glutamic acid in a continuous oscillatory baffled crystallizer. Org. Process Res. Dev. 19, 1903–1911.

Chen, J., Sarma, B., Evans, J.M.B., Myerson, A.S., 2011. Pharmaceutical crystallization. Cryst. Growth Des. 11, 887–895.

Eder, R.J.P., Schrank, S., Besenhard, M.O., Roblegg, E., Gruber-Woelfler, H., Khinast, J.G., 2012. Continuous sonocrystallization of acetylsalicylic acid (ASA): control of crystal size. Cryst. Growth Des. 12, 4733–4738.

Günther, A., Jensen, K.F., 2006. Multiphase microfluidics: from flow characteristics to chemical and materials synthesis. Lab Chip 6, 1487–1503.

Ghiaasiaan, S.M., Abdel-Khalik, S.I., 2001. In: Garg, H.G., Hales, C.A. (Eds.), Advances in Heat Transfer: Chemistry and Biology of Hyaluronan, vol. 34. Elsevier, pp. 145–254.

Guillemet-Fritsch, S., Aoun-Habbache, M., Sarrias, J., Rousset, A., Jongen, N., Bowen, P., Lemaître, J., 2004. High-quality nickel manganese oxalate powders synthesized in a new segmented flow tubular reactor. Solid State Ionics 171, 135–140.

Hadiwinoto, G.D., Kwok, P.C.L., Tong, H.H.Y., Wong, S.N., Chow, S.F., Lakerveld, R., 2019. Integrated continuous plug-flow crystallization and spray drying of pharmaceuticals for dry powder inhalation. Ind. Eng. Chem. Res. 58, 16843–16857.

Heisel, S., Rolfes, M., Wohlgemuth, K., 2018. Discrimination between single crystals and agglomerates during the crystallization process. Chem. Eng. Technol. 41, 1218–1225.

Heisel, S., Ernst, J., Emshoff, A., Schembecker, G., Wohlgemuth, K., 2019a. Shape-independent particle classification for discrimination of single crystals and agglomerates. Powder Technol. 345, 425–437.

Heisel, S., Holtkötter, J., Wohlgemuth, K., 2019b. Measurement of agglomeration during crystallization: is the differentiation of aggregates and agglomerates via ultrasonic irradiation possible? Chem. Eng. Sci. 210, 115214.

Hohmann, L., Gorny, R., Klaas, O., Ahlert, J., Wohlgemuth, K., Kockmann, N., 2016. Design of a continuous tubular cooling crystallizer for process development on lab-scale. Chem. Eng. Technol. 39, 1268–1280.

Hohmann, L., Greinert, T., Mierka, O., Turek, S., Schembecker, G., Bayraktar, E., Wohlgemuth, K., Kockmann, N., 2018. Analysis of crystal size dispersion effects in a continuous coiled tubular crystallizer: experiments and modeling. Cryst. Growth Des. 18, 1459–1473.

Jiang, M., Braatz, R.D., 2018. Low-cost noninvasive real-time imaging for tubular continuous-flow crystallization. Chem. Eng. Technol. 41, 143–148.

Jiang, M., Braatz, R.D., 2019. Designs of continuous-flow pharmaceutical crystallizers: developments and practice. CrystEngComm 21, 3534–3551.

Jiang, M., Zhu, Z., Jimenez, E., Papageorgiou, C.D., Waetzig, J., Hardy, A., Langston, M., Braatz, R.D., 2014. Continuous-flow tubular crystallization in slugs spontaneously induced by hydrodynamics. Cryst. Growth Des. 14, 851–860.

Jiang, M., Papageorgiou, C.D., Waetzig, J., Hardy, A., Langston, M., Braatz, R.D., 2015. Indirect ultrasonication in continuous slug-flow crystallization. Cryst. Growth Des. 15, 2486–2492.

Jongen, N., et al., 2003. Development of a continuous segmented flow tubular reactor and the "Scale-out" concept – in search of perfect powders. Chem. Eng. Technol. 26, 303–305.

Kacker, R., Regensburg, S.I., Kramer, H.J., 2017. Residence time distribution of dispersed liquid and solid phase in a continuous oscillatory flow baffled crystallizer. Chem. Eng. J.

Kacker, R., Maaß, S., Emmerich, J., Kramer, H., 2018. Application of inline imaging for monitoring crystallization process in a continuous oscillatory baffled crystallizer. AIChE J. 64, 2450–2461.

Kubo, M., Kawakatsu, T., Yonemoto, T., 1998. Modelling of continuous synthesis process of TiO2 particles using slug flow tubular reactor. Chem. Eng. Res. Des. 76, 669–676.

Kudo, S., Takiyama, H., 2012. Production of fine organic crystalline particles by using milli segmented flow crystallizer. J. Chem. Eng. Jpn. 45, 305–309.

Lührmann, M.-C., Timmermann, J., Schembecker, G., Wohlgemuth, K., 2018. Enhanced product quality control through separation of crystallization phenomena in a four-stage MSMPR cascade. Cryst. Growth Des. 18, 7323–7334.

Lawton, S., Steele, G., Shering, P., Zhao, L., Laird, I., Ni, X.-W., 2009. Continuous crystallization of pharmaceuticals using a continuous oscillatory baffled crystallizer. Org. Process Res. Dev. 13, 1357–1363.

Levenstein, M.A., Wayment, L., Scott, C.D., Lunt, R., Flandrin, P.-B., Day, S.J., Tang, C.C., Wilson, C.C., Meldrum, F.C., Kapur, N., Robertson, K., 2020. Dynamic crystallization pathways of polymorphic pharmaceuticals revealed in segmented flow with inline powder X-ray diffraction. Anal. Chem. 92, 7754–7761.

Liu, Y.C., Nagy, Z.K., 2020. Continuous pharmaceutical processing. In: Nagy, Z.K., El Hagrasy, A., Litster, J. (Eds.), AAPS Advances in the Pharmaceutical Sciences Series. Springer International Publishing, Cham, pp. 129–192.

Lu, J., Litster, J.D., Nagy, Z.K., 2015. Nucleation studies of active pharmaceutical ingredients in an air-segmented microfluidic drop-based crystallizer. Cryst. Growth Des. 15, 3645–3651.
Mou, M., Jiang, M., 2020. Fast continuous non-seeded cooling crystallization of glycine in slug flow: pure alpha-form crystals with narrow size distribution. J. Pharm. Innov.
Mou, M., Li, H., Yang, B.-S., Jiang, M., 2019. Continuous generation of millimeter-sized glycine crystals in non-seeded millifluidic slug flow. Crystals 9, 412.
Nagy, Z.K., El Hagrasy, A., Litster, J. (Eds.), 2020. AAPS Advances in the Pharmaceutical Sciences Series. , 1st ed. Springer International Publishing, Cham.
Nauman, E.B., 2004. Residence time distributions. In: Handbook of Industrial Mixing: Science and Practice., pp. 1–17.
Neugebauer, P., Khinast, J.G., 2015. Continuous crystallization of proteins in a tubular plug-flow crystallizer. Cryst. Growth Des. 15, 1089–1095.
Neugebauer, P., Cardona, J., Besenhard, M.O., Peter, A., Gruber-Woelfler, H., Tachtatzis, C., Cleary, A., Andonovic, I., Sefcik, J., Khinast, J.G., 2018. Crystal shape modification via cycles of growth and dissolution in a tubular crystallizer. Cryst. Growth Des. 18, 4403–4415.
Ostermann, M.-C., Termühlen, M., Schembecker, G., Wohlgemuth, K., 2018. Growth rate measurements of organic crystals in a cone-shaped fluidized-bed cell. Chem. Eng. Technol. 41, 1165–1172.
Rasche, M.L., Jiang, M., Braatz, R.D., 2016. Mathematical modeling and optimal design of multi-stage slug-flow crystallization. Comput. Chem. Eng. 95, 240–248.
Robertson, K., Flandrin, P.-B., Klapwijk, A.R., Wilson, C.C., 2016. Design and evaluation of a mesoscale segmented flow reactor (KRAIC). Cryst. Growth Des. 16, 4759–4764.
Scheiff, F., Fluiddynamik, 2015. Stofftransport und chemische Reaktion der Suspensionskatalyse bei der Flüssig/flüssig-Pfropfenströmung in Mikrokanälen. Dissertation. Technische Universität Dortmund, Dortmund.
Su, M., Gao, Y., 2018. Air-liquid segmented continuous crystallization process optimization of the flow field, growth rate, and size distribution of crystals. Ind. Eng. Chem. Res. 57, 3781–3791.
Terdenge, L.-M., Wohlgemuth, K., 2016. Impact of agglomeration on crystalline product quality within the crystallization process chain. Cryst. Res. Technol. 51, 513–523.
Termühlen, M., Strakeljahn, B., Schembecker, G., Wohlgemuth, K., 2019. Characterization of slug formation towards the performance of air-liquid segmented flow. Chem. Eng. Sci. 207, 1288–1298.
Thulasidas, T.C., Abraham, M.A., Cerro, R.L., 1995. Bubble-train flow in capillaries of circular and square cross section. Chem. Eng. Sci. 50, 183–199.
Trachsel, F., Günther, A., Khan, S., Jensen, K.F., 2005. Measurement of residence time distribution in microfluidic systems. Chem. Eng. Sci. 60, 5729–5737.
Wang, T., Lu, H., Wang, J., Xiao, Y., Zhou, Y., Bao, Y., Hao, H., 2017. Recent progress of continuous crystallization. J. Ind. Eng. Chem. 54, 14–29.
Wang, J., Li, F., Lakerveld, R., 2018. Process intensification for pharmaceutical crystallization. Chem. Eng. Process.: Process Intensif. 127, 111–126.
Wang, Y., Su, M., Bai, Y., 2020. Mechanism of glycine crystal adhesion and clogging in a continuous tubular crystallizer. Ind. Eng. Chem. Res. 59, 25–33.
Wiedmeyer, V., Anker, F., Bartsch, C., Voigt, A., John, V., Sundmacher, K., 2017. Continuous crystallization in a helically coiled flow tube: analysis of flow field, residence time behavior, and crystal growth. Ind. Eng. Chem. Res. 56, 3699–3712.
Wittering, K., 2015. Multi-component Crystallisation in the Continuous Flow Environment. Ph.D. Thesis. University of Bath.
Wohlgemuth, K., 2012. Induced Nucleation Processes During Batch Cooling Crystallization: Zugl.: Dortmund, Techn. Univ., Diss., vol. 5., 1st ed. Schriftenreihe Anlagen - und Prozesstechnik, Verl. Dr. Hut: München.
Wood, B., Girard, K.P., Polster, C.S., Croker, D.M., 2019. Progress to date in the design and operation of continuous crystallization processes for pharmaceutical applications. Org. Process Res. Dev. 23, 122–144.
Yazdanpanah, N., Nagy, Z.K., 2020. The Handbook of Continuous Crystallization. Royal Society of Chemistry, Cambridge.
Zhang, D., Xu, S., Du, S., Wang, J., Gong, J., 2017. Progress of pharmaceutical continuous crystallization. Engineering 3, 354–364.